Characteristics of Non-Fullerene Acceptor-Based Organic Photovoltaic Active Layers Using X-ray Scattering and Solid-state NMR

Yao Wu, [†] Qin Hu, [†,‡,§] Pu Fan, [†] Yufeng Jiang, [‡] Wenkai Zhong, [‖] Weiguo Hu, *[,†] Thomas P. Russell*[,†,‡]

[†]Department of Polymer Science and Engineering, University of Massachusetts Amherst, 120 Governors Drive, Amherst, Massachusetts 01003, United States

[‡] Materials Sciences Division, Lawrence Berkeley National Laboratory, 1 Cyclotron Road, Berkeley, California 94720, United States

[§] School of Microelectronics, University of Science and Technology of China, Hefei, Anhui 230026, China

[‖]Frontiers Science Center for Transformative Molecules, In-situ Center for Physical Science, and Center of Hydrogen Science, School of Chemistry and Chemical Engineering, Shanghai Jiao Tong University, Shanghai 200240, China

Keywords: X-ray scattering; solid-state nuclear magnetic resonance; relaxation measurement; non-fullerene acceptors; organic solar cells.

ABSTRACT: With the recent development of non-fullerene acceptors, power conversion efficiencies of bulk-heterojunction organic solar cells have exceeded 18%. The morphology of the BHJ active layer, including packing, ordering, orientation, and phase behavior of the donor(s) and acceptor(s), plays critical roles in determining device performance. We characterized the morphology of active layers consisting of mixtures of PTB7/PTB7-Th (donor) and ITIC (acceptor) using grazing incidence wide-angle X-ray scattering, resonant soft X-ray scattering, and solid-state nuclear magnetic resonance (ssNMR) to correlate the morphology with device performance. PTB7-Th:ITIC has better device performance than that of PTB7:ITIC, due to smaller π-π stacking distance and smaller domain size of the phase separated morphology. One of PTB7:ITIC sample, processed from mixed solvents (chlorobenzene:benzene=1:1), shows possible partial miscibility and smaller domain size as revealed by ssNMR $T_{1\rho}$ relaxation times, which is detrimental to device performance. ssNMR results showed that ITIC could crystallize into different forms depending on processing conditions, which may have implications on the manufacturing of devices using it as an ingredient, as well as its long-term stability in service.

INTRODUCTION

Due to their promising applications as clean and renewable energy sources, bulk-heterojunction organic solar cells (OSCs), which are lightweight, transparent, and flexible,[1-6] have attracted much attention. The power conversion efficiencies (PCEs) of OSCs have undergone remarkable improvements, recently achieving values over 18% due,[7-8] primarily, to the advent of non-fullerene acceptors (NFAs).[9-18] Numerous NFAs have been designed and synthesized, overcoming the drawbacks of fullerene-derivative acceptors, including low absorption in the visible region, difficulty in changing the energy levels, and ease of aggregation in the active layer.[19-22]

Most high efficient NFAs are fused-ring electron acceptors [23], containing a rigid aromatic fused-ring core substituted with aryl and/or alkyl side chains, coupled with two strong electron-accepting groups.[24] The fused rings of the electron acceptors contain thiophene or benzene rings, which are similar to the benzodithiophene(BDT)-based electron donor materials, such as PTB7, PTB7-Th, and PM6.[25-27] The similarities in the chemical composition of the donors and NFAs limit current methods based on electron densities or refractive indices to discern details of the morphology. [28-30]

Solid-state nuclear magnetic resonance (ssNMR) is sensitive to local chemical and physical environments from the chemical bond level up to tens of nanometers, useful for probing ordering, segmental conformation, phase separation, and molecular dynamics.[31-33] Indicators, including nucleus-independent chemical shifts (NICS) due to π-π stacking[34-36] and differences in peak

shapes and $T_{1\rho}$ relaxation times between crystalline and amorphous signals, have been used to access morphological details. [37-40] ^{1}H spin diffusion can probe the state of mixing in bulk-heterojunction active layers.[41-43] Comprehensive comparisons between X-ray scattering, ssNMR and thermal methods were applied to understand the ordering behavior and state of mixing between polymer donor and fullerene acceptors in organic photovoltaic materials.[44-45]

Despite the rapid development of NFA-based OSCs in recent years, the morphology of polymer donors blended with NFAs has not been extensively studied by ssNMR.[46-47] Recently, several studies examined the local ordering at the segmental level and donor:NFAs π-π interactions based on some high efficiency donor:NFAs systems,[48-51] which were detected by ^{1}H, ^{13}C or ^{19}F ssNMR and their correlation spectra. Nguyen and coworkers used ^{1}H and ^{19}F MAS NMR spectra and their correlation spectra to investigate PTB7-Th, IOTIC, and IOTIC-4F. The degree of local order can be estimated by linewidth analysis. Correlation spectra can provide the information of the interaction between the nuclei. The increased local ordering and π-π interactions of PTB7-Th:IOTIC-4F explain the superior charge transport and extraction properties.[48] They also used solid-state ^{19}F MAS NMR and 2D $^{19}F\{^{19}F\}$ correlation spectra to detect the morphology of PM6 and Y6, which shows lack of interaction between PM6 and Y6 within a 1 nm distance.[49] In addition, they used 2D ^{13}C–^{1}H HETCOR spectra intermolecular ^{13}C–^{1}H proximities between PM6 and Y6 molecules in different low molecular weight fraction blends.[50] Zhan and coworkers used ^{19}F NMR to detect PM6, Y6, PhI-Th and $PC_{71}BM$. Linewidth analysis was performed to understand the ordering of the quaternary OPV system.[51]

In the present report, we use a representative molecule, 2,2′-[[6,6,12,12-tetrakis(4-hexylphenyl)-6,12-dihydrodithieno[2,3-d:2′,3′-d′]-s-indaceno[1,2-b:5,6-b′]dithiophene-2,8-diyl]bis[methylidyne(3-oxo-1H-indene-2,1(3H)-diylidene)]]bis[propanedinitrile] (ITIC) as an NFA, blended with a polymer donor Poly({4,8-bis[(2-ethylhexyl)oxy]benzo[1,2-b:4,5-b′]dithiophene-2,6-diyl}{3-fluoro-2-[(2-ethylhexyl)carbonyl]thieno[3,4-b]thiophenediyl}) (PTB7) or Poly([2,6′-4,8-di(5-ethylhexylthienyl)benzo[1,2-b;3,3-b]dithiophene]{3-fluoro-2[(2-ethylhexyl)carbonyl]thieno[3,4-b]thiophenediyl}) (PTB7-Th), to fabricate OSC devices. The objective of these studies is to use multiple techniques to probe the morphology and highlight the advantages and disadvantages of each and to provide caveats encountered in the comparison of the results on sample prepared in different way to develop a coherent morphological description. The PTB7-Th:ITIC based devices show an average PCE of 5.81%, which is better than that obtained for PTB7:ITIC (3.61%), even though the chemical structure of PTB7 and PTB7-Th are quite similar. In addition to absorption, charge transport, which depends on the morphology of the donor and acceptor, is critical for device performance. Morphology results of neat or blend PTB7, PTB7-Th, and ITIC samples were obtained by a range of characterization methods, including grazing incidence wide-angle X-ray scattering (GIWAXS), resonant soft X-ray scattering (RSoXS), and ssNMR. With GIWAXS, molecule ordering and orientation of each component from the neat and blend films could be obtained. With RSoXS, the phase separation behavior of the blend film was studied. With ssNMR, ordering information was obtained from by ^{13}C ssNMR peak positions, while phase separation was studied by $T_{1\rho}$ relaxation times. By

comparing the results from these methods, the morphologies of active layers with different combinations of PTB7, PTB7-Th, and ITIC were obtained, providing insights into the structure-property-performance relationship of the active layer.

RESULTS AND DISCUSSION

Photovoltaic Properties. OSC devices were fabricated with a configuration of ITO/PEDOT:PSS/active layer/PDINO[52]/Ag using PTB7 or PTB7-Th as the donor and ITIC as the acceptor. Table 1 summarizes the performance of PTB7:ITIC and PTB7-Th:ITIC devices and the related *J*-*V* curves are shown in Figure 2. The PTB7:ITIC devices have an open-circuit voltage (V_{OC}) of 0.795 V, a short-circuit current (J_{SC}) of 8.99 mA cm^{-2}, a fill factor (FF) of 52.3 %, and a PCE of 3.73 %. The PTB7-Th:ITIC based devices have a V_{OC} of 0.779 V, a J_{SC} of 14.35 mA cm^{-2}, a FF of 54.4 %, and a PCE of 6.09 %. The performance of the PTB7-Th:ITIC based devices is lower than those of previous report (6.80%, dichlorobenzene as solvent), mainly due to the different solvent in the process.[9] The PTB7-Th:ITIC devices show similar V_{OC}'s, and slightly higher FFs, and significantly higher J_{SC} values than those of PTB7:ITIC. The HOMO level of PTB7-Th is slightly higher than that of PTB7 (Fig S1 and Table S1), but they show similar V_{OC} in the devices, indicating the energy loss of PTB7-Th:ITIC is lower. The J_{SC} of OSCs is affected by many factors, including absorption of the donor and acceptor, charge transport in bulk or between interfaces, and the morphology of the active layer. PTB7:ITIC and PTB7-Th:ITIC show similar absorption in blend films (Fig S1), indicating the absorption may not affect J_{SC} in this system. PTB7-Th shows better hole mobility than PTB7, which will affect device performance.[25-26, 53] The

network morphology formed by the donor and acceptor also influences charge transport in the pure phases or at the D/A interfaces, thus device performance. We note that the efficiencies of these devices are far from being the highest performers, but the intent of this work is to determine a detailed morphology-performance relationship to provide guidance for device fabrication in general.

Grazing Incidence Wide-Angle X-Ray Scattering. GIWAXS was used to investigate molecular orientation and packing of PTB7, PTB7-Th, and ITIC neat or blend films processed by spin-coating or solution casting routes.[54] Two-dimensional GIWAXS diffraction profiles and linear cuts of the profiles are shown in Figure 3 and Figure S1.

Spin-coated PTB7 shows a strong (100) reflection at 0.36 $Å^{-1}$ in the in-plane direction and a π-π stacking peak at 1.68 $Å^{-1}$ in the out-of-plane direction. Spin-coated PTB7-Th shows a strong (100) peak at 0.30 $Å^{-1}$ in the in-plane direction and a π-π stacking peak at 1.67 $Å^{-1}$ in the out-of-plane direction. Both PTB7 and PTB7-Th have similar diffraction patterns and positions due to similar chemical structures. The crystallinity and ordering of the spin-coated ITIC films are poor due to the steric hindrance of the tetrahexylphenyl groups as peripheral substituents of the coplanar backbone. A weak (100) reflection at 0.35 $Å^{-1}$ in the in-plane direction and a π-π stacking peak at 1.48 $Å^{-1}$ in the out-of-plane direction are observed. These correspond to d-spacings of 17.95 Å, characterizing the average separation distance between adjacent alkyl chains, and 4.25 Å, characterizing the average π-π stacking distance between the rigid backbones, respectively. Spin-coated PTB7-Th neat film shows a slightly larger (100) d-spacing of 20.9 Å

than the 17.5 Å of PTB7 due to the thiophene groups on the side chains. Spin-coated PTB7 and PTB7-Th neat films have similar π-π stacking distances of 3.74 and 3.76 Å, respectively, indicating that the thiophene group on the side chains does not affect the packing of the backbones in the spin-coated films. The d-spacing of π-π stacking peak of the spin-coated ITIC neat film is 4.25 Å, much shorter than those of PTB7 and PTB7-Th, due to the restriction in the packing of backbones from the tetrahexylphenyl groups on the side chains.

In the spin-coated blend films, both the (100) peaks in the in-plane direction of the donors remain in the same position, indicating the addition of ITIC does not change the packing of the donors. The (100) peak of ITIC merges with the (100) peak of the donors, making it difficult to distinguish whether ITIC persists or, possibly, co-crystallizes with the donors. The π-π stacking peaks of PTB7:ITIC and PTB7-Th:ITIC in the out-of-plane direction are located at 1.75 $Å^{-1}$ and 1.60 $Å^{-1}$, respectively. In comparison to the π-π stacking peaks of the neat films, PTB7:ITIC shows a slightly closer packing distance of 3.59 Å, in comparison to the 3.74 Å distance for PTB7, while that for PTB7-Th:ITIC increases from 3.76 Å to 3.93 Å. The position of scattering peaks in the spin-coating samples are similar to those reported results.[9, 55-57] We also calculated the coherence length from the Scherrer equation[58], $Lc = 2\pi K/\Delta q$, where Δq is the full-width at half-maximum (FWHM) of the reflection and K is a shape factor (0.9 was used here), evaluating the crystalline size of the (100) peaks of the donors. The FWHMs of the in-plane (100) peaks for PTB7, PTB7:ITIC, PTB7-Th and PTB7-Th:ITIC are 0.186 $Å^{-1}$, 0.127 $Å^{-1}$, 0.190 $Å^{-1}$ and 0.184 $Å^{-1}$, respectively. The coherence lengths of the (100) reflections for PTB7 and PTB7:ITIC are

30.5 Å and 44.6 Å, while the coherence lengths of the (100) reflections PTB7-Th and PTB7-Th:ITIC are 29.7 Å to 30.7 Å. PTB7:ITIC blend film has larger coherence lengths than that of PTB7-Th:ITIC, although PTB7 and PTB7-Th has similar coherence length, which is due to the addition of ITIC. Usually, a smaller π-π stacking distance and larger coherence length would increase the carrier hopping between the molecules, thus enhance charge transport in bulk. However, the highly ordered structure tends to pack into larger domain, which is unfavorable for exciton dissociation at D/A interfaces.

It is worthwhile to compare the morphological features from the spin-coated and as-cast films in order to connect the detailed molecular information afforded by ssNMR (obtained from as-cast films) to thin films used for devices (obtained from spin-coated films). Recognizing differences in the structures and morphologies under these different preparation conditions is essential in transferring information obtained on thicker films, used to get sufficient material to run NMR, to performance results obtained on the thinner films used in devices obtained by spin coating or blades coating. As-cast PTB7 shows a weak (100) peak at 0.32 $Å^{-1}$ in the in-plane direction with a π-π stacking peak at 1.43 $Å^{-1}$ in the out-of-plane direction. As-cast PTB7-Th shows a strong (100) peak at 0.28 $Å^{-1}$ in in-plane direction and a π-π stacking peak at 1.63 $Å^{-1}$ in the out-of-plane direction. The as-cast PTB7 and PTB7-Th are characterized by larger (100) and π-π stacking distances when compared to the same materials that have been spin-coated. The as-cast ITIC shows multiple reflections at 0.36 $Å^{-1}$ and 0.44 $Å^{-1}$ in the in-plane direction and at 0.52 $Å^{-1}$ in the out-of-plane direction, indicating the formation of different crystals during slow solvent

evaporation. For the as-cast blend films, the peaks of ITIC are retained in both the in-plane and out-of-plane directions. The coherent lengths of the reflection at 0.52 $Å^{-1}$ for ITIC, PTB7:ITIC and PTB7-Th:ITIC are 119, 192 and 133 Å, respectively. The addition of PTB7 promotes the crystalline of ITIC, resulting in larger crystal sizes, while the addition of PTB7-Th has negligible effects. In contrast to the spin-coated samples, all the as-cast ITIC-containing samples show enhanced crystallinity due to the promotion of crystal growth during the slow solvent evaporation. Scattering profiles of as-cast samples in different azimuthal angles is shown in Fig S7. In as-cast ITIC, the (100) peaks at 0.36 $Å^{-1}$ arise at low azimuthal angles, while the peaks at 0.52 $Å^{-1}$ only arise at high azimuthal angles, indicating the orientation of ITIC. When ITIC blend with PTB7 or PTB7-Th, the orientation of ITIC still retains due to the same trend of two peaks.

Resonant Soft X-Ray Scattering. RSoXS at the carbon edge was used to investigate the phase separation behavior of PTB7:ITIC and PTB7-Th:ITIC blend films. The scattering profiles are shown in Fig 3. The detailed fittings to determine the scattering peaks are shown in Fig S3. The domain size of the mixture can be estimated from the correlation length and the volume fractions of the components. The average domain sizes were calculated from the position of peak 2 by $d = \pi/q$. The peak 2 in the fitting reveals mesoscale phase separation and dominates in the scattering profiles.[59] The scattering peaks for PTB7:ITIC SP, PTB7:ITIC AC, PTB7-Th:ITIC SP and PTB7:ITIC AC are 0.0050, 0.0019, 0.0063 and 0.0034 $Å^{-1}$, respectively. The average domain sizes of PTB7:ITIC and PTB7-Th:ITIC spin-coated blend films are ~63 and ~50nm, respectively. The average domain sizes of PTB7-Th:ITIC is a little larger than that of previous report (33 nm,

inverted device, ZnO in the bottom), due to the different transporting layer in the bottom of the devices.[55] The larger coherent length of PTB7:ITIC was observed by GIWAXS, meaning that the increased ordering tends to form larger domain sizes. Excitons, generated after light absorption, must diffuse to D/A interfaces to dissociate into holes and electrons before recombination. Typical exciton diffusion lengths are several tens of nanometers for organic materials and the domain sizes of PTB7:ITIC and PTB7-Th:ITIC are on the outer limits of the exciton diffusion length, giving rise to low J_{sc} and FF values of the OSC devices. In comparison to the spin-coated blend films, as-cast samples have larger average domain sizes ~165 nm for PTB7:ITIC and ~92nm for PTB7-Th:ITIC due to the enhanced ordering and stronger phase separation behavior between two domains. The widths of the interface between the domains, determined from a Porod analysis of the data at higher scattering vectors, are relatively sharp at 2.6 and 3.6 nm for the spin-coated and as-cast PTB7:ITIC films, respectively. The interfacial widths of the spin-coated and as-cast PTB7-Th:ITIC films are 2.0 and 2.7 nm, respectively. Interestingly, the interfacial widths for the as-cast films are larger than those for the spin-coated films, even though the ordering also increases.

Solid-State Nuclear Magnetic Resonance. Due to the large amount of sample required (30 – 50 mg) to generate sufficient signal, all ssNMR studies were conducted on as-cast samples. Spin-coating films are produced with fast solvent evaporation and high shear rate. Their morphologies are likely metastable and could evolve during usage when exposed to various light and thermal environments.[60] The morphologies of as-cast samples are more stable, being

produced in more thermodynamically-favored conditions. Therefore, studies of as-cast samples may offer useful perspective toward the understanding of the morphological evolution of active layers. Figure 4 shows the CP/MAS ^{13}C ssNMR spectrum of PTB7, PTB7-Th, and ITIC as-received samples. The chemical structure of PTB7 and PTB7-Th are very similar, only with a thiophene substituting the oxygen atom on the benzodithiophene (BDT) side chains in PTB7-Th, resulting in very similar ssNMR spectra for PTB7 and PTB7-Th. The peaks between 10 and 45 ppm are assigned to the 2-ethylhexyl side chains, while the signals between 105 and 160 ppm arise from the BDT or thieno[3,4-b]thiophene. The resonance at 76 ppm, not present for PTB7-Th, arises from the carbon of the 2-ethylhexyl side chains connected to the ether group of PTB7. For ITIC, the peaks between 10 and 40 ppm are attributed to the alkyl chains, while the peaks above 110 ppm are from the conjugated backbones. The peaks at 11 and 41ppm are unique to PTB7 and PTB7-Th, while the peaks at 36 and 140 ppm are unique to ITIC. Those signals are minimally overlapped with signals from the other component in the blend and can be used to track relaxation behavior in each ingredient. Most of the small signals between 60 and 90 ppm and above 170 ppm are spinning sidebands of the backbone signals.

There seemed to be no significant change of morphology for PTB7 and PTB7-Th upon solvent processing, as evidenced by the similar peak shapes and positions for as-received and as-cast films (Figure S2). Interestingly, the ssNMR spectra of the as-received and as-cast ITIC are different, particularly in the aromatic region, which likely suggests that they have different crystalline lattice geometries.

Figure 5 shows CP/MAS ^{13}C ssNMR spectra of as-cast ITIC and its blends with PTB7/PTB7-Th. The ITIC signals in PTB7:ITIC and PTB7-Th:ITIC show the same positions in the ssNMR spectrum, suggesting that the ITIC in both blends have the same crystal forms, which are consistent with the GIWAXS results of the as-cast films. Benzene has lower boiling point than that of chlorobenzene, which may induce smaller domain sizes during the coating process due to its faster evaporation. Both donor and acceptor can also maintain good solubility in benzene. Mixed solvents (chlorobenzene:benzene=1:1) were also used to process PTB7:ITIC films, named PTB7:ITIC*, which shows different peak positions for the ITIC component, indicating that its crystal form was different from the that in the other PTB7:ITIC blend. This suggests the possible role of solvent in influencing the morphology of the film. This result is confirmed by WAXS (Fig S3). PTB7:ITIC* shows a peak at 0.45 $Å^{-1}$ that is slightly more intense than that of PTB7:ITIC, indicating the ordering of PTB7:ITIC and PTB7:ITIC* are slightly different.

Miscibility between donor and acceptor can be probed by ^{1}H spin diffusion. During ^{1}H T_1 and $T_{1\rho}$ relaxations, ^{1}H spin diffusion occurs between neighboring domains, which results in the averaging of the relaxation times between them. Due to severe signal overlap, relatively low signal-to-noise ratios, and low contrast of dynamics between the donor and acceptor, we chose to study the change of T_1 and $T_{1\rho}$ relaxation times rather than using the classical method of creating a magnetization gradient at the beginning of the spin diffusion process to probe miscibility. If the relaxation times of donor and acceptor in the blends differ from those in their respective neat

films, domain size information can be qualitatively inferred.

As the backbones of both the donors and acceptors in the present study are rigid, the driving force of the relaxations arises from the dynamics of the side chains. The side chains of the acceptor ITIC are linear alkyl chains, which primarily exhibit a fast crankshaft-type rotational mode (~ 10^9 s^{-1}), while those of the donors are branched and thus have an additional slower mode of rotation around the methine carbon (~ 10^5 s^{-1}), providing a significant driving force for $T_{1\rho}$ relaxation.

T_1 and $T_{1\rho}$ relaxation times of each component in the blends were measured by ^{13}C detection, tracking the decays of the signals not overlapping with the other component. $T_{1\rho}$ of the donors and acceptors in various neat and blend films are listed in Table 2. Several observations can be made: First, the $T_{1\rho}$ values of different peaks of the same component are similar, despite each moiety exhibiting different dynamics, indicating that the spin diffusion during spinlock within the same molecule is efficient. Second, for the blend samples PTB7:ITIC and PTB7-Th:ITIC, both of which were prepared with chlorobenzene, $T_{1\rho}$ values are very similar to each other, suggesting reproducibility of the processing condition. A related observation is that the $T_{1\rho}$ relaxation times of PTB7 and PTB7-Th for different processing conditions are similar, suggesting that their physical states are less susceptible to processing conditions. Third, the ITIC component in various neat and blend films show a wide variation of $T_{1\rho}$. This could be due to the different crystalline forms and/or populations within the ITIC phase, as the dynamics of the side chains would be different in the amorphous and the various crystalline phases due to different packing.

Finally, $T_{1\rho}$ of donors and acceptors differ significantly except for sample PTB7:ITIC* prepared in mixed solvent (chlorobenzene:benzene=1:1). This is due to (1) their different side-chain structures, which result in their different intrinsic $T_{1\rho}$, as discussed above; and (2) the spatial separation between donor and acceptor is beyond the reach of spin diffusion. The only exception is sample PTB7:ITIC*, to be discussed in more detail below.

As the strength of ^{1}H-^{1}H dipolar coupling is attenuated during spin lock, spin diffusion may be more affected by magic angle spinning. To investigate this effect, $T_{1\rho}$ relaxation times were measured on a PTB7 sample under several spinning speeds. The results are shown in Table S1. Since the backbone moieties lack dynamics, their intrinsic $T_{1\rho}$ are expected to be long, possibly greater than 20 ms. The methyl groups of the side chains exhibit high-speed rotations ($> 10^9$ s^{-1}) and their intrinsic $T_{1\rho}$s are also expected to be long. However, the experimentally measured values for all the moieties are within 30% of each other for all spinning speeds, suggesting relatively efficient spin diffusion within the same molecule. The $T_{1\rho}$ of the backbone aromatic protons and the methyl groups of the side chains, on the other hand, are still longer than those of other side-chain protons for all the spinning speeds, indicating that within several milliseconds, spin diffusion cannot completely average out $T_{1\rho}$ times for all the moieties within the same molecule. The differences increase with increasing spinning speed due to more substantial attenuation of the ^{1}H-^{1}H dipolar coupling by magic-angle spinning.

^{1}H T_1 of the donors and acceptors in the neat and blend films are shown in Table S2. Several observations can be made from these data. The T_1 of ITIC in various neat and blend films vary

between 0.6 and 1.7 s. which is likely due to variations of crystalline forms and/or crystallinity. The T_1 of PTB7 in its various neat and blend films are very similar, suggesting that the physical state of PTB7 is relatively insensitive to processing conditions. This result is consistent with the observation from the $T_{1\rho}$ and the peak positions data. The T_1 of PTB7 and PTB7-Th are very similar, which is to be expected as it is a result of their identical side-chain chemical structures.

Since ^1H T_1 of ITIC is highly dependent on its morphology, and some ITIC samples have ^1H T_1's that are very similar to those of PTB7 and PTB7-Th, ^1H T_1 is not a suitable independent method to study miscibility between ITIC and PTB7/PTB7-Th. However, the $T_{1\rho}$ of ITIC in all the samples are significantly different from those of PTB7 and PTB7-Th. Therefore, $T_{1\rho}$ appears to be a more useful tool to probe miscibility. The disadvantages of using $T_{1\rho}$ are that spin diffusion during $T_{1\rho}$ relaxation is slower than that during T_1 relaxation, & and $T_{1\rho}$ relaxations are usually fast, often shorter than 20 ms, which means that spin diffusion would not have much time to reach far, likely less than 5 nm.

For sample PTB7:ITIC* prepared in mixed solvent, the $T_{1\rho}$ of ITIC is the shortest among all samples shown in Table 2, while the $T_{1\rho}$ of PTB7 is longest among all samples. The difference between the $T_{1\rho}$ of ITIC and PTB7 components for this sample is the smallest among all the blend samples. These results suggest that there is likely a partial miscibility between ITIC and PTB7. Although the short $T_{1\rho}$ of ITIC in this sample could be due to other factors, such as a smaller crystallinity, such an alteration of dynamical behavior as compared to its neat state is most likely due to the disturbance introduced by the presence of PTB7 in a close proximity

(likely < 10 nm).

Assessment of the crystallinity of non-fullerene acceptors is challenging for GIWAXS due to the broad diffraction peaks and for ssNMR due to the severe signal overlap. ^{1}H T_1 relaxation times might offer some insights here. As the crystalline domains of acceptors are expected to be small (e.g., < 20 nm), the crystalline and amorphous components of an acceptor are expected to have the same ^{1}H T_1, due to efficient spin diffusion, as is the case for most semicrystalline polymers. The apparent T_1 will be the weighted average of the intrinsic T_1's of the crystalline and amorphous fractions. Therefore, the variations of T_1 of ITIC as observed in Table S2 are likely due to variations of crystallinity, from which crystallinity information may be extracted. A detailed study of this problem would be of future interest.

Comparing X-ray scattering and ssNMR data, we find that the ordering behavior of neat PTB7 and PTB7-Th is insensitive to process conditions, showing similar peak positions in GIWAXS and ssNMR spectra under different processing conditions. Neat ITIC, on the other hand, shows process-dependent ordering. As-cast ITIC has numerous reflections in the GIWAXS and sharper peaks in the backbone region of the ssNMR, indicating an enhanced ordering during solvent casting. The ordering of ITIC increases upon blending with PTB7, as observed by GIWAXS, though the ssNMR does not show distinct changes, which is likely due to its insensitivity to longer-range order. As-cast ITIC show obvious orientation in both pure and blend samples by GIWAXS, which cannot be detected by ssNMR due to the random orientation of the film samples in the rotor. $T_{1\rho}$ of PTB7:ITIC* suggests a likely partial miscibility of the

components (<10 nm), which is detrimental to device performance (Fig 4. and Table S4), due to low carrier mobility between D/A interfaces.

CONCLUSIONS

We fabricated organic solar cells base on PTB7/PTB7-Th:ITIC, which show standard device performance. The morphology of PTB7/PTB7-Th:ITIC pure or blend films processed in different conditions were investigated by GIWAXS, RSoXS and ssNMR. GIWAXS is a tool to understand the molecular ordering and orientation of the films. PTB7 and PTB7-Th show similar molecular ordering under different process conditions. X-ray diffraction showed that the crystallinity of ITIC was higher for the as-cast samples than the spin-coating ones. The addition of PTB7 also promotes the crystallization of ITIC. RSoXS is used to investigate the phase separation behavior of blend films. The as-cast samples have larger domain sizes than those of spin-coated samples, due to slow solvent evaporation. The domain size of PTB7:ITIC is larger than that of PTB7-Th:ITIC, which lowers the device performance. CP/MAS ssNMR measurements revealed polymorphism of ITIC in both neat and blend films. Miscibility between donor and acceptor was probed by ^{1}H spin diffusion. $T_{1\rho}$ relaxation for PTB7:ITIC*, prepared with a chlorobenze/benzene mixed solvent, showed partial miscibility between ITIC and PTB7, which likely contributed to a lower device performance.

ASSOCIATED CONTENT

SUPPORTING INFORMATION

The Supporting Information is available free of charge on the ACS Publications website. Detailed experimental procedures including materials, characterization, device fabrication and additional characterization data, such as GIWAXS, RSoXS and ssNMR.

AUTHOR INFORMATION

Corresponding Author

*Email: weiguoh@umass.edu; russell@mail.pse.umass.edu

ORCID

Yao Wu: 0000-0002-6680-7347

Weiguo Hu: 0000-0002-7868-1657

Thomas P. Russell: 0000-0001-6384-5826

Notes

The authors declare no competing financial interest.

ACKNOWLEDGMENTS

The authors were supported by Office of Naval Research, under Contract N00014-17-1-2241. Portions of this research were conducted at beamline 7.3.3 and 11.0.1.2 of Advanced Light Source, Materials Science Division, The Molecular Foundry, Lawrence Berkeley National Laboratory, which is supported by the Office of Science, Office of Basic Energy Sciences, of the U.S. Department of Energy under Contract No. DE-AC02-05CH11231.

REFERENCES

(1) Cheng, Y.-J.; Yang, S.-H.; Hsu, C.-S., Synthesis of Conjugated Polymers for Organic

Solar Cell Applications. *Chem. Rev.* **2009,** *109*, 5868-5923.

(2) Li, G.; Zhu, R.; Yang, Y., Polymer solar cells. *Nat. Photon.* **2012,** *6*, 153-161.

(3) Lu, L.; Zheng, T.; Wu, Q.; Schneider, A. M.; Zhao, D.; Yu, L., Recent Advances in Bulk Heterojunction Polymer Solar Cells. *Chem. Rev.* **2015,** *115*, 12666-12731.

(4) Wu, Y.; Liu, Y.; Emrick, T.; Russell, T. P., Polymer design to promote low work function surfaces in organic electronics. *Prog. Polym. Sci.* **2020,** *103*, 101222.

(5) Page, Z. A.; Liu, Y.; Duzhko, V. V.; Russell, T. P.; Emrick, T., Fulleropyrrolidine interlayers: Tailoring electrodes to raise organic solar cell efficiency. *Science* **2014,** *346*, 441-444.

(6) Meng, L.; Zhang, Y.; Wan, X.; Li, C.; Zhang, X.; Wang, Y.; Ke, X.; Xiao, Z.; Ding, L.; Xia, R.; Yip, H.-L.; Cao, Y.; Chen, Y., Organic and solution-processed tandem solar cells with 17.3% efficiency. *Science* **2018,** *361*, 1094-1098.

(7) Liu, Q. S.; Jiang, Y. F.; Jin, K.; Qin, J. Q.; Xu, J. G.; Li, W. T.; Xiong, J.; Liu, J. F.; Xiao, Z.; Sun, K.; Yang, S. F.; Zhang, X. T.; Ding, L. M., 18% Efficiency organic solar cells. *Sci. Bull.* **2020,** *65*, 272-275.

(8) Zhang, M.; Zhu, L.; Zhou, G.; Hao, T.; Qiu, C.; Zhao, Z.; Hu, Q.; Larson, B. W.; Zhu, H.; Ma, Z.; Tang, Z.; Feng, W.; Zhang, Y.; Russell, T. P.; Liu, F., Single-layered organic photovoltaics with double cascading charge transport pathways: 18% efficiencies. *Nat. Commun.* **2021,** *12*, 309.

(9) Lin, Y.; Wang, J.; Zhang, Z. G.; Bai, H.; Li, Y.; Zhu, D.; Zhan, X., An electron acceptor challenging fullerenes for efficient polymer solar cells. *Adv. Mater.* **2015,** *27*, 1170-4.

(10) Wu, Y.; Bai, H.; Wang, Z.; Cheng, P.; Zhu, S.; Wang, Y.; Ma, W.; Zhan, X., A planar electron acceptor for efficient polymer solar cells. *Energy Environ. Sci.* **2015,** *8*, 3215-3221.

(11) Kan, B.; Feng, H.; Wan, X.; Liu, F.; Ke, X.; Wang, Y.; Wang, Y.; Zhang, H.; Li, C.; Hou, J.; Chen, Y., Small-Molecule Acceptor Based on the Heptacyclic Benzodi(cyclopentadithiophene) Unit for Highly Efficient Nonfullerene Organic Solar Cells. *J. Am. Chem. Soc.* **2017,** *139*, 4929-4934.

(12) Zhao, W.; Li, S.; Yao, H.; Zhang, S.; Zhang, Y.; Yang, B.; Hou, J., Molecular Optimization Enables over 13% Efficiency in Organic Solar Cells. *J. Am. Chem. Soc.* **2017,** *139*, 7148-7151.

(13) Baran, D.; Ashraf, R. S.; Hanifi, D. A.; Abdelsamie, M.; Gasparini, N.; Rohr, J. A.; Holliday, S.; Wadsworth, A.; Lockett, S.; Neophytou, M.; Emmott, C. J.; Nelson, J.; Brabec, C. J.; Amassian, A.; Salleo, A.; Kirchartz, T.; Durrant, J. R.; McCulloch, I., Reducing the efficiency-stability-cost gap of organic photovoltaics with highly efficient and stable small molecule acceptor ternary solar cells. *Nat. Mater.* **2017,** *16*, 363-369.

(14) Cheng, P.; Zhang, M.; Lau, T.-K.; Wu, Y.; Jia, B.; Wang, J.; Yan, C.; Qin, M.; Lu, X.; Zhan, X., Realizing Small Energy Loss of 0.55 eV, High Open-Circuit Voltage > 1 V and High Efficiency > 10% in Fullerene-Free Polymer Solar Cells via Energy Driver. *Adv. Mater.* **2017,** *29*, 1605216.

(15) Zheng, Z.; Hu, Q.; Zhang, S.; Zhang, D.; Wang, J.; Xie, S.; Wang, R.; Qin, Y.; Li,

W.; Hong, L.; Liang, N.; Liu, F.; Zhang, Y.; Wei, Z.; Tang, Z.; Russell, T. P.; Hou, J.; Zhou, H., A Highly Efficient Non-Fullerene Organic Solar Cell with a Fill Factor over 0.80 Enabled by a Fine-Tuned Hole-Transporting Layer. *Adv. Mater.* **2018,** *30*, 1801801.

(16) Yuan, J.; Zhang, Y.; Zhou, L.; Zhang, G.; Yip, H.-L.; Lau, T.-K.; Lu, X.; Zhu, C.; Peng, H.; Johnson, P. A.; Leclerc, M.; Cao, Y.; Ulanski, J.; Li, Y.; Zou, Y., Single-Junction Organic Solar Cell with over 15% Efficiency Using Fused-Ring Acceptor with Electron-Deficient Core. *Joule* **2019,** *3*, 1140-1151.

(17) Jia, B.; Wang, J.; Wu, Y.; Zhang, M.; Jiang, Y.; Tang, Z.; Russell, T. P.; Zhan, X., Enhancing the Performance of a Fused-Ring Electron Acceptor by Unidirectional Extension. *J. Am. Chem. Soc.* **2019,** *141*, 19023-19031.

(18) Li, T.; Wu, Y.; Zhou, J.; Li, M.; Wu, J.; Hu, Q.; Jia, B.; Pan, X.; Zhang, M.; Tang, Z.; Xie, Z.; Russell, T. P.; Zhan, X., Butterfly Effects Arising from Starting Materials in Fused-Ring Electron Acceptors. *J. Am. Chem. Soc.* **2020,** *142*, 20124-20133.

(19) Yan, C.; Barlow, S.; Wang, Z.; Yan, H.; Jen, A. K. Y.; Marder, S. R.; Zhan, X., Non-fullerene acceptors for organic solar cells. *Nat. Rev. Mater.* **2018,** *3*, 18003.

(20) Hou, J.; Inganas, O.; Friend, R. H.; Gao, F., Organic solar cells based on non-fullerene acceptors. *Nat. Mater.* **2018,** *17*, 119-128.

(21) Zhang, J.; Tan, H. S.; Guo, X.; Facchetti, A.; Yan, H., Material insights and challenges for non-fullerene organic solar cells based on small molecular acceptors. *Nat. Energy* **2018,** *3*, 720-731.

(22) Cheng, P.; Li, G.; Zhan, X.; Yang, Y., Next-generation organic photovoltaics based on non-fullerene acceptors. *Nat. Photon.* **2018,** *12*, 131-142.

(23) Wang, J.; Zhan, X., Fused-Ring Electron Acceptors for Photovoltaics and Beyond. *Acc Chem Res* **2021,** *54*, 132-143.

(24) Lin, Y.; Li, T.; Zhao, F.; Han, L.; Wang, Z.; Wu, Y.; He, Q.; Wang, J.; Huo, L.; Sun, Y.; Wang, C.; Ma, W.; Zhan, X., Structure Evolution of Oligomer Fused-Ring Electron Acceptors toward High Efficiency of As-Cast Polymer Solar Cells. *Adv. Energy Mater.* **2016,** *6*, 1600854.

(25) Liang, Y.; Xu, Z.; Xia, J.; Tsai, S. T.; Wu, Y.; Li, G.; Ray, C.; Yu, L., For the bright future-bulk heterojunction polymer solar cells with power conversion efficiency of 7.4%. *Adv. Mater.* **2010,** *22*, 135-8.

(26) Liao, S. H.; Jhuo, H. J.; Cheng, Y. S.; Chen, S. A., Fullerene derivative-doped zinc oxide nanofilm as the cathode of inverted polymer solar cells with low-bandgap polymer (PTB7-Th) for high performance. *Adv. Mater.* **2013,** *25*, 4766-71.

(27) Zhang, M.; Guo, X.; Ma, W.; Ade, H.; Hou, J., A Large-Bandgap Conjugated Polymer for Versatile Photovoltaic Applications with High Performance. *Adv. Mater.* **2015,** *27*, 4655-60.

(28) Liu, F.; Gu, Y.; Shen, X.; Ferdous, S.; Wang, H.-W.; Russell, T. P., Characterization of the morphology of solution-processed bulk heterojunction organic photovoltaics. *Prog. Polym. Sci.* **2013,** *38*, 1990-2052.

(29) Huang, Y.; Kramer, E. J.; Heeger, A. J.; Bazan, G. C., Bulk heterojunction solar cells: morphology and performance relationships. *Chem. Rev.* **2014,** *114*, 7006-43.

(30) Diao, Y.; Zhou, Y.; Kurosawa, T.; Shaw, L.; Wang, C.; Park, S.; Guo, Y.; Reinspach, J. A.; Gu, K.; Gu, X.; Tee, B. C.; Pang, C.; Yan, H.; Zhao, D.; Toney, M. F.; Mannsfeld, S. C.; Bao, Z., Flow-enhanced solution printing of all-polymer solar cells. *Nat. Commun.* **2015,** *6*, 7955.

(31) Brown, S. P.; Spiess, H. W., Advanced Solid-State NMR Methods for the Elucidation of Structure and Dynamics of Molecular, Macromolecular, and Supramolecular Systems. *Chem. Rev.* **2001,** *101*, 4125-4156.

(32) Laws, D. D.; Bitter, H.-M. L.; Jerschow, A., Solid-State NMR Spectroscopic Methods in Chemistry. *Angew. Chem. Int.* **2002,** *41*, 3096-3129.

(33) Seifrid, M.; Reddy, G. N. M.; Chmelka, B. F.; Bazan, G. C., Insight into the structures and dynamics of organic semiconductors through solid-state NMR spectroscopy. *Nat. Rev. Mater.* **2020,** *5*, 910-930.

(34) Dudenko, D.; Kiersnowski, A.; Shu, J.; Pisula, W.; Sebastiani, D.; Spiess, H. W.; Hansen, M. R., A strategy for revealing the packing in semicrystalline pi-conjugated polymers: crystal structure of bulk poly-3-hexyl-thiophene (P3HT). *Angew. Chem. Int.* **2012,** *51*, 11068-72.

(35) Baltisberger, J. H.; Walder, B. J.; Keeler, E. G.; Kaseman, D. C.; Sanders, K. J.; Grandinetti, P. J., Communication: Phase incremented echo train acquisition in NMR spectroscopy. *J. Chem. Phys.* **2012,** *136*, 211104.

(36) Seifrid, M. T.; Reddy, G. N. M.; Zhou, C.; Chmelka, B. F.; Bazan, G. C., Direct Observation of the Relationship betweenMolecular Topology and Bulk Morphology for a pi-Conjugated Material. *J. Am. Chem. Soc.* **2019,** *141*, 5078-5082.

(37) Mafra, L.; Santos, S. M.; Siegel, R.; Alves, I.; Paz, F. A.; Dudenko, D.; Spiess, H. W., Packing interactions in hydrated and anhydrous forms of the antibiotic Ciprofloxacin: a solid-state NMR, X-ray diffraction, and computer simulation study. *J. Am. Chem. Soc.* **2012,** *134*, 71-4.

(38) Nieuwendaal, R. C.; Snyder, C. R.; DeLongchamp, D. M., Measuring Order in Regioregular Poly(3-hexylthiophene) with Solid-State13C CPMAS NMR. *ACS Macro Lett.* **2014,** *3*, 130-135.

(39) Karki, A.; Wetzelaer, G. J. A. H.; Reddy, G. N. M.; Nádaždy, V.; Seifrid, M.; Schauer, F.; Bazan, G. C.; Chmelka, B. F.; Blom, P. W. M.; Nguyen, T. Q., Unifying Energetic Disorder from Charge Transport and Band Bending in Organic Semiconductors. *Adv. Funct. Mater.* **2019,** *29*, 1901109.

(40) Shen, X.; Hu, W.; Russell, T. P., Measuring the Degree of Crystallinity in Semicrystalline Regioregular Poly(3-hexylthiophene). *Macromolecules* **2016,** *49*, 4501-4509.

(41) Nieuwendaal, R. C.; Snyder, C. R.; Kline, R. J.; Lin, E. K.; VanderHart, D. L.; DeLongchamp, D. M., Measuring the Extent of Phase Separation in Poly-3-Hexylthiophene/Phenyl-C61-Butyric Acid Methyl Ester Photovoltaic Blends with1H Spin Diffusion NMR Spectroscopy. *Chem. Mater.* **2010,** *22*, 2930-2936.

(42) Schneider, H.; Saalwächter, K.; Roos, M., Complex Morphology of the Intermediate Phase in Block Copolymers and Semicrystalline Polymers As Revealed by 1H NMR Spin Diffusion Experiments. *Macromolecules* **2017,** *50*, 8598-8610.

(43) Chen, Q.; Schmidt-Rohr, K., Measurement of the local 1H spin-diffusion coefficient in polymers. *Solid State Nucl. Magn. Reson.* **2006,** *29*, 142-52.

(44) Miller, N. C.; Cho, E.; Junk, M. J.; Gysel, R.; Risko, C.; Kim, D.; Sweetnam, S.; Miller, C. E.; Richter, L. J.; Kline, R. J.; Heeney, M.; McCulloch, I.; Amassian, A.; Acevedo-Feliz, D.; Knox, C.; Hansen, M. R.; Dudenko, D.; Chmelka, B. F.; Toney, M. F.; Bredas, J. L.; McGehee, M. D., Use of X-ray diffraction, molecular simulations, and spectroscopy to determine the molecular packing in a polymer-fullerene bimolecular crystal. *Adv. Mater.* **2012,** *24*, 6071-9.

(45) Graham, K. R.; Cabanetos, C.; Jahnke, J. P.; Idso, M. N.; El Labban, A.; Ngongang Ndjawa, G. O.; Heumueller, T.; Vandewal, K.; Salleo, A.; Chmelka, B. F.; Amassian, A.; Beaujuge, P. M.; McGehee, M. D., Importance of the donor:fullerene intermolecular arrangement for high-efficiency organic photovoltaics. *J. Am. Chem. Soc.* **2014,** *136*, 9608-18.

(46) Nieuwendaal, R. C.; Ro, H. W.; Germack, D. S.; Kline, R. J.; Toney, M. F.; Chan, C. K.; Agrawal, A.; Gundlach, D.; VanderHart, D. L.; Delongchamp, D. M., Measuring Domain Sizes and Compositional Heterogeneities in P3HT-PCBM Bulk Heterojunction Thin Films with 1H Spin Diffusion NMR Spectroscopy. *Adv. Funct. Mater.* **2012,** *22*, 1255-1266.

(47) Nieuwendaal, R. C.; DeLongchamp, D. M.; Richter, L. J.; Snyder, C. R.; Jones, R. L.; Engmann, S.; Herzing, A.; Heeney, M.; Fei, Z.; Sieval, A. B.; Hummelen, J. C., Characterization of Interfacial Structure in Polymer-Fullerene Bulk Heterojunctions via ^{13}C {^{2}H} Rotational Echo Double Resonance NMR. *Phys. Rev. Lett.* **2018,** *121*, 026101.

(48) Karki, A.; Vollbrecht, J.; Dixon, A. L.; Schopp, N.; Schrock, M.; Reddy, G. N. M.; Nguyen, T. Q., Understanding the High Performance of over 15% Efficiency in Single-Junction Bulk Heterojunction Organic Solar Cells. *Adv. Mater.* **2019,** *31*, 1903868.

(49) Karki, A.; Vollbrecht, J.; Gillett, A. J.; Selter, P.; Lee, J.; Peng, Z.; Schopp, N.; Dixon, A. L.; Schrock, M.; Nádaždy, V.; Schauer, F.; Ade, H.; Chmelka, B. F.; Bazan, G. C.; Friend, R. H.; Nguyen, T. Q., Unifying Charge Generation, Recombination, and Extraction in Low-Offset Non-Fullerene Acceptor Organic Solar Cells. *Adv. Energy Mater.* **2020,** *10*, 2001203.

(50) Karki, A.; Vollbrecht, J.; Gillett, A. J.; Xiao, S. S.; Yang, Y.; Peng, Z.; Schopp, N.; Dixon, A. L.; Yoon, S.; Schrock, M.; Ade, H.; Reddy, G. N. M.; Friend, R. H.; Nguyen, T.-Q., The role of bulk and interfacial morphology in charge generation, recombination, and extraction in non-fullerene acceptor organic solar cells. *Energy Environ. Sci.* **2020,** *13*, 3679-3692.

(51) Zhang, W.; Huang, J.; Xu, J.; Han, M.; Su, D.; Wu, N.; Zhang, C.; Xu, A.; Zhan, C., Phthalimide Polymer Donor Guests Enable over 17% Efficient Organic Solar Cells via Parallel-Like Ternary and Quaternary Strategies. *Adv. Energy Mater.* **2020,** *10*, 2001436.

(52) Zhang, Z.-G.; Qi, B.; Jin, Z.; Chi, D.; Qi, Z.; Li, Y.; Wang, J., Perylene diimides: a thickness-insensitive cathode interlayer for high performance polymer solar cells. *Energy Environ. Sci.* **2014,** *7*, 1966.

(53) Cui, C.; Wong, W.-Y.; Li, Y., Improvement of open-circuit voltage and photovoltaic properties of 2D-conjugated polymers by alkylthio substitution. *Energy Environ. Sci.* **2014,** *7*, 2276-2284.

(54) Muller-Buschbaum, P., The active layer morphology of organic solar cells probed with grazing incidence scattering techniques. *Adv. Mater.* **2014,** *26*, 7692-709.

(55) Yi, X. P.; Gautam, B.; Constantinou, I.; Cheng, Y.; Peng, Z. H.; Klump, E. X.; Ba, X. C.; Ho, C. H. Y.; Dong, C.; Marder, S. R.; Reynolds, J. R.; Tsang, S. W.; Ade, H.; So, F., Impact of Nonfullerene Molecular Architecture on Charge Generation, Transport, and Morphology in PTB7-Th-Based Organic Solar Cells. *Adv. Funct. Mater.* **2018,** *28*, 1802702.

(56) Guo, S.; Ning, J.; Körstgens, V.; Yao, Y.; Herzig, E. M.; Roth, S. V.; Müller-Buschbaum, P., The Effect of Fluorination in Manipulating the Nanomorphology in PTB7:PC71BM Bulk Heterojunction Systems. *Adv. Energy Mater.* **2015,** *5*, 1401315.

(57) Song, L.; Wang, W.; Barabino, E.; Yang, D.; Korstgens, V.; Zhang, P.; Roth, S. V.; Muller-Buschbaum, P., Composition-Morphology Correlation in PTB7-Th/PC71BM Blend Films for Organic Solar Cells. *ACS Appl Mater Interfaces* **2019,** *11*, 3125-3135.

(58) Rivnay, J.; Noriega, R.; Kline, R. J.; Salleo, A.; Toney, M. F., Quantitative analysis of lattice disorder and crystallite size in organic semiconductor thin films. *Phys. Rev. B* **2011,** *84*, 045203.

(59) Ma, W.; Tumbleston, J. R.; Ye, L.; Wang, C.; Hou, J.; Ade, H., Quantification of nano- and mesoscale phase separation and relation to donor and acceptor quantum efficiency, J(sc), and FF in polymer:fullerene solar cells. *Adv. Mater.* **2014,** *26*, 4234-41.

(60) Cheng, P.; Zhan, X., Stability of organic solar cells: challenges and strategies. *Chem Soc Rev* **2016,** *45*, 2544-82.

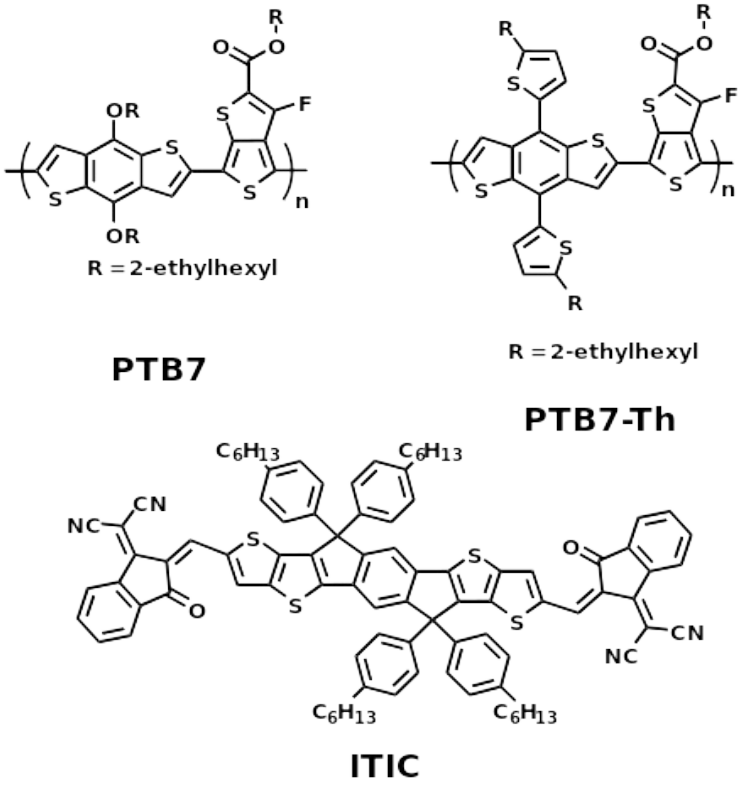

Scheme 1. Chemical structure of PTB7, PTB7-Th, and ITIC.

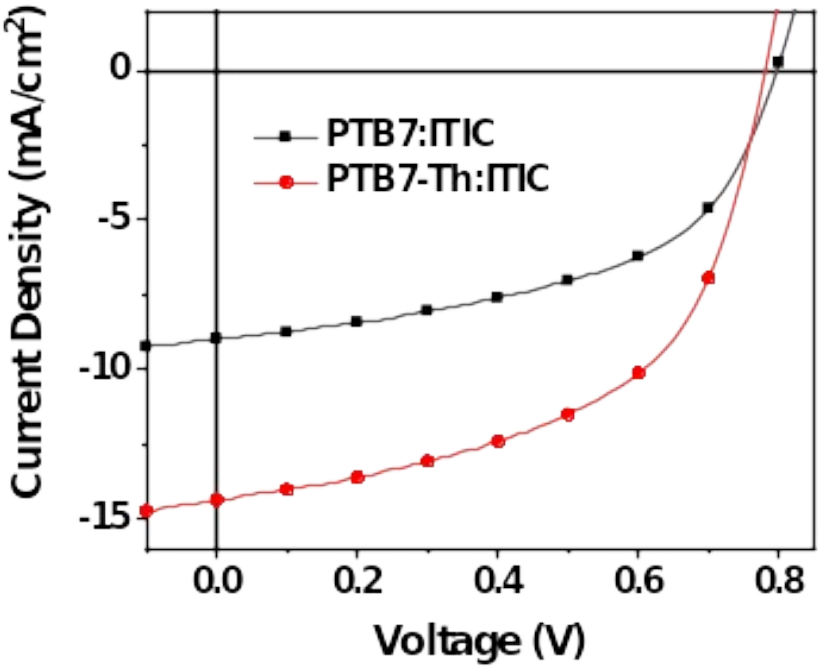

Figure 1. *J*–*V* curves of optimized devices based on PTB7:ITIC and PTB7-Th:ITIC.

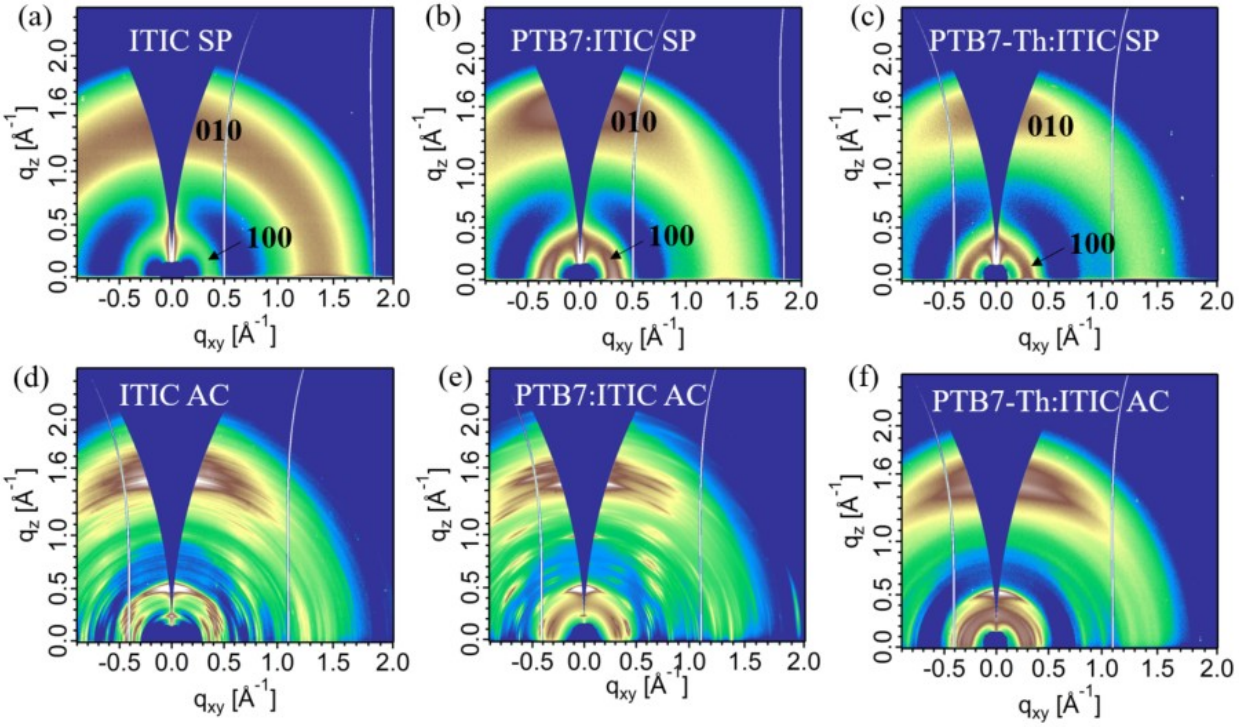
(a)
ITIC SP
010
100
(b)
PTB7:ITIC SP
010
100
(c)
PTB7-Th:ITIC SP
010
100
(d)
ITIC AC
(e)
PTB7:ITIC AC
(f)
PTB7-Th:ITIC AC
q_z [Å^{-1}]
q_{xy} [Å^{-1}]
0.0 0.5 1.0 1.6 2.0
-0.5 0.0 0.5 1.0 1.5 2.0

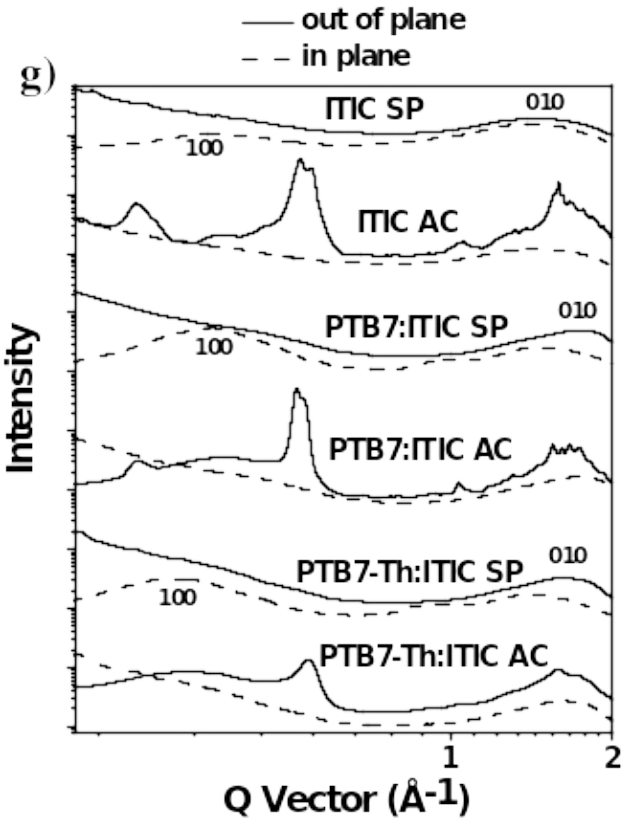

Figure 2. 2D GIWAXS patterns of a) ITIC SP, b) PTB7:ITIC SP, c) PTB7-Th:ITIC SP, d) ITIC AC, e) PTB7:ITIC AC and f) PTB7-Th:ITIC AC; g) scattering profiles of in-plane and out-of-plane for ITIC, PTB7:ITIC and PTB7-Th:ITIC. SP:spin-coating; AC: as-cast.

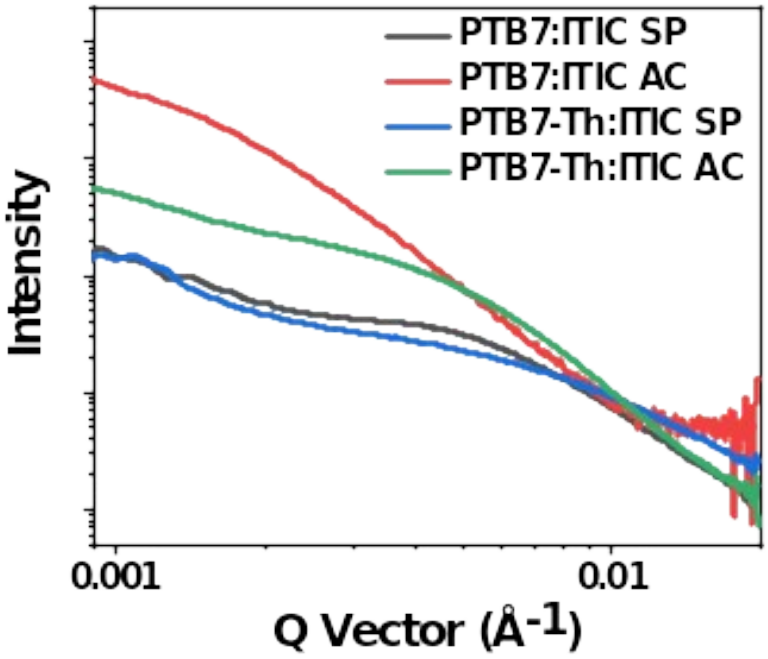

Figure 3. RSoXS profiles of PTB7:ITIC and PTB7-Th:ITIC blend films. SP:Spin-coating; AC: As-cast.

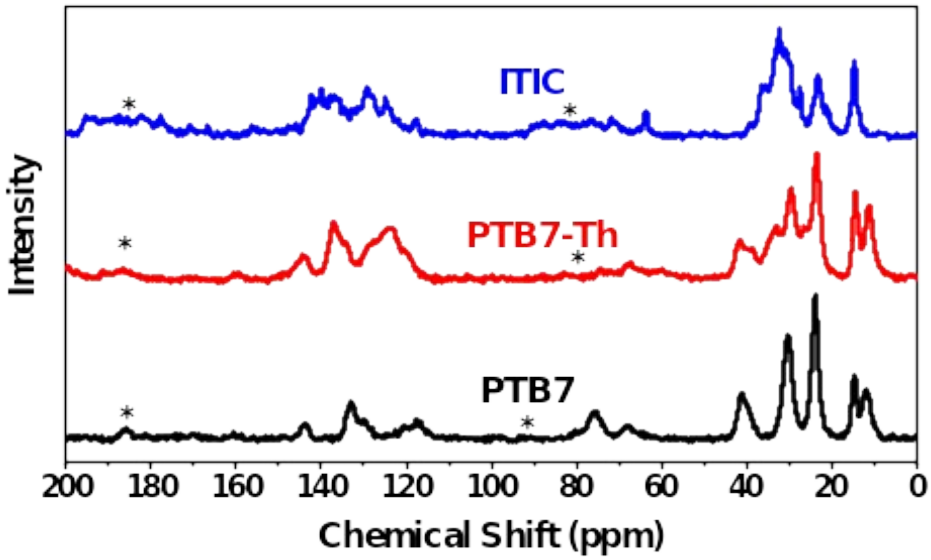

Figure 4. The CP/MAS ^{13}C ssNMR spectrum of PTB7, PTB7-Th, and ITIC as received samples. Spinning sidebands are marked with a "*".

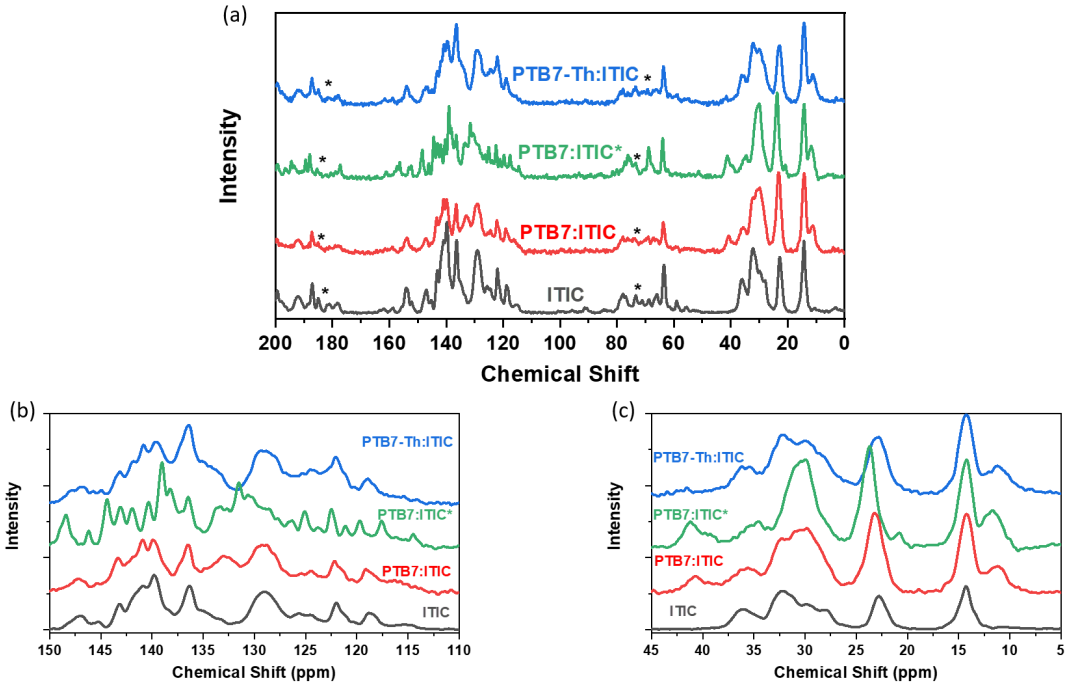

Figure 5. (a) The CP/MAS ^{13}C ssNMR full spectrum and amplified spectrum in the (b) aromatic region or (c) aliphatic region of ITIC PTB7:ITIC, PTB7:ITIC* and PTB7-Th:ITIC as-cast samples. Spinning sidebands are marked with a black "*".

Table 1. Performance of the Optimized OSC Devices Based on PTB7:ITIC and PTB7-Th:ITIC.

Active layer	V_{OC}[a] (V)	J_{SC}[a] (mA cm^{-2})	FF[a] (%)	PCE[a] (%)
PTB7:ITIC	0.797±0.001 (0.795)	8.74±0.24 (8.99)	51.8±1.2 (52.3)	3.61±0.07 (3.73)
PTB7-Th:ITIC	0.783±0.002 (0.779)	14.05±0.21 (14.35)	52.8±0.4 (54.4)	5.81±0.04 (6.09)

[a] Average values with standard deviations were obtained from over 10 devices. The values in parentheses are the parameters from the best device.

Table 2. $T_{1\rho}$ relaxation times (ms) of as-cast PTB7, PTB7-Th, and ITIC in the neat and blend films. All the decays were fitted with single-exponential models. The error bars are 1-sigma fitting errors.

	Donor[a]					Acceptor[b]		
Samples/ms	11 ppm	24 ppm	41 ppm	124 ppm	133 ppm	23 ppm	36 ppm	140 ppm
PTB7	3.5±0.2	2.8±0.1	2.5±0.1		3.5±0.2			
PTB7-Th		1.3±0.1		2.3±0.2				
PTB7:ITIC	3.9±0.1		2.9±0.1				11.2±0.8	15.3±0.3
PTB7:ITIC*	4.9±0.5		3.0±0.2				5.7±0.6	7.8±0.4
PTB7-Th:ITIC	3.3±0.2		1.4±0.2				10.9±0.9	13.4±0.2
ITIC						9.5±0.6	9.3±0.4	10.8±0.3

[a] The signals are from PTB7 or PTB7-Th; [b] The signals are from ITIC. PTB7:ITIC* was processed from mixed solvent (chlorobenzene:benzene=1:1); Other samples were processed from pure chlorobenzene.

Table of content